Draft version February 23, 2017
Preprint typeset using LaTeX style AASTeX6 v. 1.0

arXiv:1702.06545v1 [astro-ph.GA] 21 Feb 2017

HOW TO DETECT INCLINED WATER MASER DISKS (AND POSSIBLY MEASURE BLACK HOLE MASSES)

Jeremy Darling
Center for Astrophysics and Space Astronomy, Department of Astrophysical and Planetary Sciences, University of Colorado, 389 UCB, Boulder, CO 80309-0389, USA

ABSTRACT

We describe a method to identify inclined water maser disks orbiting massive black holes and to potentially use them to measure black hole masses. Due to the geometry of maser amplification pathways, the minority of water maser disks are observable: only those viewed nearly edge-on have been identified, suggesting that an order of magnitude additional maser disks exist. We suggest that inward-propagating masers will be gravitationally deflected by the central black hole, thereby scattering water maser emission out of the disk plane and enabling detection. The signature of an inclined water maser disk would be narrow masers near the systemic velocity that appear to emit from the black hole position, as identified by the radio continuum core. To explore this possibility, we present high resolution (0.07″–0.17″) Very Large Array line and continuum observations of 13 galaxies with narrow water maser emission and show that three are good inclined disk candidates (five remain ambiguous). In the best case, for CGCG 120−039, we show that the maser and continuum emission are coincident to within 3.5 ± 1.4 pc (6.7 ± 2.7 milliarcsec). Subsequent very long baseline interferometric maps can confirm candidate inclined disks and have the potential to show maser rings or arcs that provide a direct measurement of black hole mass, although the mass precision will rely on knowledge of the size of the maser disk.

Keywords: accretion, accretion disks — galaxies: nuclei — gravitational lensing: strong — masers — radiation mechanisms: non-thermal — radio lines: galaxies

1. INTRODUCTION

Water masers arising from thin disks around massive black holes provide high brightness temperature non-thermal dynamical tracers of gas in Keplerian orbits. As such, water maser disks viewed edge-on provide tracers of the Keplerian potential and enable measurement of the black hole mass, provided a distance is known in order to translate the apparent angular disk size into a physical size (e.g., Miyoshi et al. 1995). Maser accelerations and proper motions can also be observed, and because the circular velocity is known from Doppler shifts, the geometric distance to the black holes (and host galaxies) can be determined (e.g., Herrnstein et al. 1998). Geometric distances obtained from water masers provide a crucial independent measurement of the Hubble constant and can be used to calibrate other distance indicators such as the period-luminosity relation of Cepheids (Riess et al. 2016).

These measurements require maser disks that are viewed within a few degrees of edge-on: otherwise, maser beaming directs emission away from the observer because masers propagate along velocity-coherent paths through the disk. For thin disks, this propagation occurs along the radial path along the line of sight toward the black hole and along the disk tangent points. For warped disks, such as that found in NGC 4258, the picture is more nuanced because a warped disk provides numerous sightlines and inclinations that intersect velocity-coherent parts of the disk (Humphreys et al. 2013). Nonetheless, inclined maser disks are generally not seen in water maser surveys. Or are they?

It seems likely that inclined water maser disks have already been detected by single dish surveys, but they have been discarded because they show no high velocity lines that have canonically been used to identify maser disks. In this paper, we propose a mechanism to produce detectable maser emission from inclined disks that may also be used to obtain black hole masses (Section 2), we present a method to detect inclined maser disks based on extant surveys (Section 3), we present Karl G. Jansky Very Large Array (VLA)[1] observations of candidate

jdarling@colorado.edu

[1] The National Radio Astronomy Observatory is a facility of the

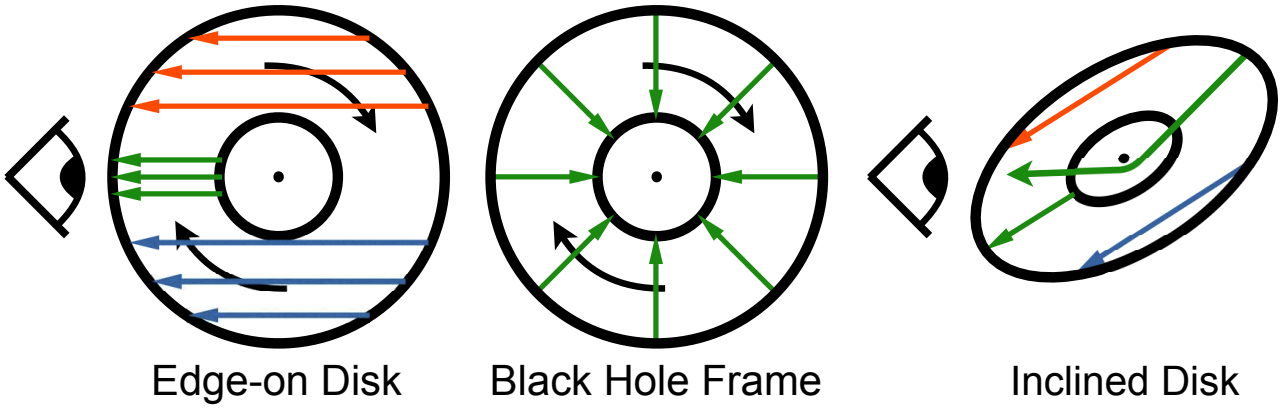

Figure 1. Maser amplification pathways for Keplerian disks orbiting massive black holes. These diagrams are schematic and not to scale. Left: the geometry of an egde-on rotating disk showing systemic velocity masers (green) and high-velocity redshifted (red) and blueshifted (blue) masers at the tangent points of the disk. Center: in the black hole rest frame, all disk motion is perpendicular to the radial direction, providing velocity-coherent amplification pathways at the systemic velocity (or rest frame). In-going (and out-going) radial masers will populate the disk in this reference frame. Right: In-going masers may be gravitationally lensed/deflected by the central black hole into the sightline of an observer who would not otherwise see maser emission from an inclined disk. Only the systemic velocity masers would be seen by this observer, and they will appear to arise from the location of the black hole. High-resolution imaging might reveal a ring or arc of water maser emission, providing a black hole mass measurement.

inclined disks (Sections 4 and 5), and we provide a list of inclined disk candidates for further study (Sections 6 and 7). In what follows, we assume a flat cosmology with parameters $H_0 = 70$ km s^{-1} Mpc^{-1}, $\Omega_M = 0.27$, and $\Omega_\Lambda = 0.73$, and we calculate distances from redshifts in the CMB rest frame.

2. A THOUGHT EXPERIMENT

Consider a typical 22 GHz water maser thin disk in Keplerian orbit around a massive black hole. This thin disk shows systemic velocity masers at the center of the observed disk, along a radial amplification path, and it shows high-velocity red- and blue-shifted masers at the tangent points of the disk, along azimuthal paths, amplifying spontaneous emission and background host galaxy continuum (Figure 1, left). If a thin disk is inclined by more than a few degrees, the masers are no longer beamed toward the observer and the disk would not be detected. The known water maser disks show an inclination typically within $\sim$5° of edge-on (e.g., Kuo et al. 2011), suggesting that an order of magnitude additional maser disks exist, and they are simply beamed in directions we cannot observe. Note that the famous water maser disk in NGC 4258 (e.g., Miyoshi et al. 1995; Herrnstein et al. 1998) is atypical, with a disk inclination of 72°, but the disk warp provides sightlines that are nearly edge-on, and this is where the masers are seen (Humphreys et al. 2013).

For the following discussion we will use fiducial parameters similar to those of many of the known maser disks (Kuo et al. 2011; Greene et al. 2016). We assume a distance of 10 Mpc, a black hole mass of $M_{BH} = 10^7\ M_\odot$ (and therefore a Schwarzschild radius of $R_s \sim 1\ \mu$pc), and a circular rotation speed of 1000 km s^{-1} in the maser-active part of the disk located 0.5 pc from the black hole and spanning 0.2 pc. We assume a disk thickness equal to that of NGC 4258: 5.5×10^{14} cm or 0.18 mpc (1σ; Argon et al. 2007).

Consider how this system appears to an observer at the location of the black hole: the disk describes a plane in the sky. Water masers reaching this observer must be purely radial (propagating inward) but will have a coherent amplification path in all radial directions (Figure 1, center). All Keplerian Doppler shifts will be across the line of sight, so all maser emission reaching this location will have zero velocity in this reference frame (ignoring the transverse Doppler shift, which is negligible at $\sim$2 km s^{-1}). The black hole-frame observer will thus see a ring of maser light or maser spots with low velocity spread. The maser-active part of the disk would subtend $\sim$2.5 arcminutes (1σ). The expected maser opening angle would be similar, $\sim$3 arcminutes, assuming a maser path-to-size ratio of $\sim$0.2 pc/0.2 mpc $\simeq$ 1000, implying maser light spanning $\sim$500 R_s at the black hole.

The black hole Kerr metric would thus be bathed in maser light with a continuous distribution of impact parameters, implying gravitational deflection of maser light into nearly all angles (the deflection at 100 R_s is 1.1° and grows inversely with impact parameter R as $\theta = 2R_s/R$; Einstein (1915)). One would therefore expect incoming maser light to be scattered into many angles, representing a gravitational lensing de-focusing of a given incoming beam. But portions of multiple

National Science Foundation operated under cooperative agreement by Associated Universities, Inc.

maser beams from around the disk may be deflected into a given direction, making the net flux as a function of angular direction uncertain and in need of numerical modeling.

NGC 4258 has a warped disk (e.g., Humphreys et al. 2013), which means that the in-going radial masers can be misaligned and thus be beamed above or below the dynamical center of the disk, and that the continuous distribution of disk inclination angles will fully populate the black hole metric volume with beams from multiple angles, further enhancing the sampling of impact parameters and deflection angles. If warped disks are common, then maser disks with high velocity lines will be detected more often than one would assume based on random inclination alone (in other words, parts of many disks will have inclinations appropriate for detectable maser amplification), and the black hole will be illuminated by in-going masers from above and below the nominal disk plane, producing a range of incoming maser impact parameters and angles with respect to the disk, thereby enhancing the gravitational deflection probability toward any given observer. Regardless of whether disks are warped or not, maser light will be scattered away from the maser disk plane, making inclined disks potentially detectable, but likely faint compared to edge-on disk masers.

Masers amplify seed photons, and these seed photons can be the portion of a radio continuum that matches the maser line frequency, appropriately Doppler-shifted, or they can be spontaneously emitted maser line photons. In known maser disks, the systemic radial masers typically amplify the AGN radio continuum, and the high-velocity tangential masers amplify spontaneous emission or possibly radio continuum from the host galaxy itself. In-going radial masers do not have access to AGN seed photons and must amplify either continuum from the host galaxy or inward-directed spontaneous emission from the outer parts of the disk. In either case, it is reasonable to expect in-going masers to be weaker than the out-going systemic masers from edge-on disks. It is unclear how the amplification of in-going masers would compare to the amplification of the high-velocity masers in edge-on disks because the tangential amplification pathway may or may not have a physically longer or higher column density velocity-coherent path for amplification.

If one were to observe a water maser disk from a direction other than edge-on, would water maser emission be seen? The thought experiment described here suggests that it would, and the inclination of the disk with respect to the observer would select the deflection angle (or equivalently the impact parameter) of the observed maser light. For example, deflection by 10° would allow observation of masers from the back side of a disk with an inclination of 80°, requiring an impact parameter of 12 R_s. Other parts of the disk could be viewed if light reaches smaller impact parameters. If, as expected, there is a continuous range of impact parameters, then a continuous distribution of maser light from an extended portion of the disk will contribute to a spectrally narrow maser line complex seen by the observer at nearly any inclination (but perhaps with higher likelihood and intensity at higher inclinations).

2.1. *Observable Signatures*

The observational signatures of an inclined water maser disk would be:

1. A narrow line or line complex
2. at the systemic velocity
3. at the apparent black hole location.

The black hole location would be indicated by the radio continuum core, ideally observed at the same frequency as the water maser. The observational signatures of an inclined water maser disk, however, may also arise from other mechanisms. Water masers can be produced in radio jet-molecular cloud interactions (e.g., Gallimore et al. 1996; Claussen et al. 1998; Peck et al. 2003; Henkel et al. 2005), in star-forming regions (e.g., Tarchi et al. 2002a,b; Henkel et al. 2005; Hofner et al. 2006; Darling et al. 2008; Brogan et al. 2010; Darling 2011; Tarchi et al. 2011b; Amiri & Darling 2016), and in outflows (e.g., Greenhill et al. 2003b; Kondratko et al. 2005; Tarchi et al. 2011a, but note that some objects in the latter survey may be candidates for inclined disk masers). These are likely to be the main contaminant among an inclined disk survey sample. VLBI identification of the maser with an AGN via spatial coincidence with the core radio continuum — identified by the spectral index — can resolve the ambiguity (Section 5).

In contrast to edge-on disk systemic masers, it is unclear whether inclined disk maser lines will show proper motion or acceleration. This may depend on the clumpiness of maser-emitting regions, on the maser beam sizes, on the physical extent of the disk that is sampled by the observed line, and on the deflection angle to the observer. One might expect lensed masers to show little or no time variability, but the substructure seen in known water maser disks and the natural variability of water masers suggests that this may be a bad assumption.

Many extragalactic water masers detected in previous surveys meet some or all of the above observational criteria: inclined water maser disks may have already been detected! In most cases, when a single systemic velocity line is detected in water maser surveys, there is no interferometric follow-up because distance or black hole mass measurements (traditionally) require edge-on disks, the signature of which are the high velocity lines emitted from the tangent points of the disk. High res-

olution observations may also be frustrated by weak or variable water masers.

In Section 4 we present interferometric mapping of a sample of narrow-line systemic velocity water masers that appear to be inclined disk maser candidates. If observations show that the masers remain unresolved and are centered at the location of the central massive black hole (as identified by simultaneous radio continuum observations at 20 GHz), then they remain candidates and should be mapped with VLBI.

2.2. *Black Hole Masses*

The Einstein radius of a strong gravitational lens is

$$\theta_E = \sqrt{2R_s \frac{D_{LS}}{D_L D_S}} = 9.2 \sqrt{\frac{R_s}{\mathrm{mpc}} \frac{D_{LS}}{\mathrm{pc}}} \left(\frac{D_L}{\mathrm{Mpc}}\right)^{-1} \mathrm{mas}, \quad (1)$$

where D_L, D_S, and D_{LS} are the angular diameter distances to the lens, to the source, and between the lens and the source, respectively, and $D_L \simeq D_S$ for the black hole-maser disk configuration (after Einstein 1936). For the fiducial parameters listed above ($R_s = 1$ μpc, $D_{LS} = 0.5$ pc, and $D_L = 10$ Mpc), $2\theta_E = 0.041$ mas. Since the angular resolution (HPBW) of the Very Long Baseline Array (VLBA) is 0.3 milliarcseconds at 22.2 GHz (which should be compared to twice the Einstein radius), the Einstein radius for the fiducial maser disk and black hole would require space-based VLBI to resolve. On the other hand, terrestrial VLBI could resolve a water maser Einstein ring for a more massive black hole with a physically larger maser disk: for $R_s = 100$ μpc ($M_{BH} = 10^9$ $M_\odot$), $D_{LS} = 2$ pc, and $D_L = 10$ Mpc, $2\theta_E = 0.82$ mas. Unfortunately, water maser disks have yet to be identified orbiting 10^9 $M_\odot$ black holes, but it is unclear whether is this a selection effect or a consequence of physics (van den Bosch et al. 2016). The most massive black hole measured using a water maser disk to date is in NGC 1194 with $M_{BH} = 10^{7.85\pm0.05}$ $M_\odot$ (Kuo et al. 2011; Greene et al. 2016).

Were an Einstein ring observable from a back side ingoing maser in an edge-on disk or from an in-going maser from an edge-on portion of an inclined warped disk, then one can infer a black hole mass from the angular size of the ring. One does need independent measurements of the luminosity distance to the black hole (D_L) and the size of the maser-emitting disk (D_{LS}). D_L can be obtained from an assumed cosmology and the cosmological redshift, but D_{LS} may be more difficult to measure. The precision of black hole masses obtained from this method may be limited by our ability to measure, model, or estimate the radius of the maser-emitting part of the disk.

Einstein rings require linear alignment between the source, the lens, and the observer, which is not germane to the inclined maser disk geometry (for unwarped disks). Instead, one would naïvely expect to see multiple images of the same maser, which can also be related to the black hole mass. This expectation, which is correct for isotropic emitters, is probably incorrect for masers.

An important difference between maser emission and the standard treatment of gravitational lensing is maser beaming: while there may be sightlines in a gravitational lens geometry that land on the emitter, emission may not be seen if light is not beamed along that sightline. For a general pointlike isotropic light source offset from the lens by angle θ_S, there are two solutions to the lens equation:

$$\theta_\pm = \frac{1}{2}\left(\theta_S \pm \sqrt{\theta_S^2 + 4\theta_E^2}\right). \quad (2)$$

θ_+ represents the angle between the lens and the source image appearing outside θ_E, and θ_- represents the angle of the image appearing inside θ_E (Narayan & Bartelmann 1995, Equation 24, Figures 5 and 7). For an inclined maser disk configuration, no emission is directed significantly out of the disk plane, so no maser emission would be seen in the θ_+ direction. On the other hand, θ_- may be small enough that this sightline is included in the maser beam passing very close to the central black hole. In this case, the source-observer deflection angle α_- nearly matches the complement of the disk inclination: $\alpha_- \simeq \pi/2 - i$ (Figure 1, right).

In contrast to canonical lensing, we expect that the maser beaming will produce only one maser spot image, where light is deflected in the manner shown schematically in Figure 1 (right). This maser image will lie inside the Einstein radius. For isotropic extended emitters, this image would also be demagnified, but masers are not isotropic emitters and can be exceptionally compact (equivalently, they demonstrate high brightness temperatures). The degree of demagnification is therefore unclear and requires numerical ray-tracing to assess.

For the fiducial parameters above, and assuming an inclination of 80°, $\theta_S = (R_{\mathrm{maser}}/D_S)\sin\alpha_- = 1.8$ mas, $\theta_E = 0.021$ mas, and therefore $|\theta_-| = 0.2$ μas, which is equivalent to 11 R_s. The maser beam spans this distance from the black hole, so the maser emission can be lensed toward the observer in this case. For the 10^9 $M_\odot$ black hole with a larger maser disk described above, $\theta_S = (R_{\mathrm{maser}}/D_S)\sin\alpha_- = 7.2$ mas, $\theta_E = 0.41$ mas, and therefore $|\theta_-| = 24$ μas, which is again equivalent to 11 R_s (the impact parameter determines the deflection angle, which is determined by the inclination).

One would therefore expect lensed masers from inclined disks to be faint and appear to arise from the black hole location ($\theta_- \ll 1$ mas). This treatment assumes a single pointlike maser rather than an extended continuous disk of masers or a set of distributed maser spots. In this more realistic scenario, numerical

ray-tracing is required to connect the observable lensed maser image to the black hole mass and maser disk configuration.

Lensed masers from inclined disks may appear to be pointlike or they may describe arcs. In-going masers from the far side of an edge-on disk or in-going masers from an inclined but warped disk may produce Einstein rings. Single-epoch VLBI maps can therefore provide black hole masses, but space-based VLBI may be required for the typical $\sim 10^7\ M_\odot$ black hole associated with water maser disks. The mass measurement precision will be limited by uncertainty about the maser disk size rather than by the distance to the object (the maser will provide the systemic redshift, which can be converted into a distance, and the distance uncertainty will be dominated by peculiar velocity departures from the Hubble flow).

2.3. *Back-Side Masers in Edge-on Disks*

If there are in-going radial water masers in maser disks (and there is no compelling reason to think otherwise), then there should be systemic water masers seen in edge-on disks from the back side of the disk, both lensed and unlensed by the black hole. Are such masers in extant data?

If there are also front-side systemic masers in an edge-on disk, then they will be orders of magnitude brighter than back-side masers, even in the presence of strong lensing, simply due to amplification considerations. The front-side masers can amplify AGN radio continuum, whereas the back-side masers will either be driven by stimulated emission (but with an amplification pathway equal to the front-side masers) or by host galaxy continuum, which is substantially weaker than AGN continuum at 22 GHz in many cases. The back-side maser contribution may therefore be confused by the front-side emission, particularly since both types of maser emission will occur at the systemic velocity.

In rare cases, a back-side maser might be distinguishable from the front-side emission either by a position or a velocity offset (there is some spread to systemic velocity masers, e.g. Gao et al. (2016)). The observational signature of a back-side maser would be an acceleration in the opposite sense of the front-side systemic maser acceleration (i.e., negative acceleration under the convention that positive velocities are redshifted). This is not seen in published systemic maser acceleration measurements (e.g. Greenhill et al. 1995; Nakai et al. 1995; Braatz et al. 2010; Kuo et al. 2015; Gao et al. 2016), but such a signal could be lost amid the brighter and numerous front-side masers.

If a back-side maser is lensed into an arc or Einstein ring by the central black hole, then it might be extended in VLBI maps. Resolved systemic maser emission would therefore be an additional observable signature of back-side masers.

3. CANDIDATE SELECTION

If inclined water maser disks can be detected via gravitational lensing or deflection of in-going masers by massive black holes, then they have likely already been detected in surveys for maser disks. But they were rejected as disk candidates because they lacked high-velocity emission. Inclined maser disks will appear to have maser emission only at the systemic velocity of the galaxy or AGN. We therefore use extant water maser surveys to select inclined disk candidates.

Using extant water maser surveys, most of which favor Seyfert 2 AGN, we examined single-dish spectra compiled by the Megamaser Cosmology Project[2] to select objects showing a narrow systemic velocity maser or maser complex. We also imposed a 30 mJy line flux limit and excluded objects south of $-20°$ declination. This process identified 16 inclined maser disk candidates (Table 1), and most candidates (14) have only been observed with a single dish. Those that do have interferometric maps are NGC 3556, which was mapped using the VLA in CnB and DnA configurations (Tarchi et al. 2011b) with no 22 GHz continuum detected (1σ rms noise of $\sim$0.5 mJy beam^{-1}), and NGC 3735,which was mapped using A-array (Greenhill et al. 1997), but no 22 GHz continuum was detected.

Since the inclinations of known maser disks are nearly edge-on, the number of inclined maser disks must be large, roughly an order of magnitude larger than the number of detected maser disks. However, the gravitational lensing or deflection of detectable in-going radial masers adds substantial uncertainty to the detection expectations. We do not know how common observable lensed inclined maser disks are in the universe because we do not know the opening angle of the masers, the size of the maser spots with respect to the black hole's Schwarzschild radius, the brightness of in-going masers, which will depend on the 22 GHz seed photons from the host galaxy, or the degree of gravitational lensing demagnification.

4. OBSERVATIONS AND DATA REDUCTION

We observed the 22.23508 GHz $6_{16} - 5_{23}$ ortho water maser line and 20 GHz radio continuum toward 16 candidate inclined maser disks (see Section 3 and Table 1) using the VLA in A configuration (the highest angular resolution configuration). Observations of program 15A-297 spanned June 19 2015 through September 26 2015 in five sessions. The fifth session occurred

[2] https://safe.nrao.edu/wiki/bin/view/Main/PrivateWaterMaserList

during the A-array to D-array reconfiguration. Each session included visits to flux and bandpass calibrators, and observations of each target object were interleaved with nearby complex gain calibrators with a ∼4 minute switching cadence.

Spectral line and continuum observations were simultaneous. The spectral line observations were centered on the redshift of the host galaxy, had 1.1–1.9 km s^{-1} spectral resolution, used 1536 channels to span 128 MHz (1700–2900 km s^{-1}), and used dual circular polarization and 8-bit sampling. Continuum observations spanned 4 GHz, 18–22 GHz, using 32 spectral windows spanning 128 MHz each using 128 channels in dual circular polarization and 3-bit sampling.

Table 1 lists the details of the observations and the rms noise in the line cubes and continuum maps. Typical beam sizes were 80–100 milliarcseconds. Noise was about 3 mJy beam^{-1} in 1.2 km s^{-1} channels in the spectral line cubes and about 15–20 μJy beam^{-1} in the continuum. The exception was the $z \simeq 0.66$ water maser J0804+3607 (Barvainis & Antonucci 2005) that was redshifted to 13.4 GHz, in Ku band, which necessarily had lower angular and spectral resolution and lower rms noise in the line but higher rms continuum noise. In this case, the continuum was centered on 14 GHz and spanned 12–16 GHz.

The observing session on September 15 2015 had poor 22 GHz weather for A configuration and could not be calibrated or imaged. NGC 3359, NGC 3556, and NGC 3735 are therefore only listed in Table 1 and are not discussed further or included in any analysis of the remaining 13 objects.

All data reduction and analysis was performed using the Common Astronomy Software Applications package (CASA; McMullin et al. 2007). Calibration and flagging used a modified CASA pipeline plus additional manual flagging. Imaging used Briggs weighting with robustness 0.5. Spectra were extracted from spectral line cubes using a maser-centered beam, and integrated line maps were restricted to line-emitting channels. All spectra use the optical velocity definition in the Barycentric reference frame.

5. RESULTS

Water masers were detected in 9 out of 13 objects, and 20 GHz continuum emission was detected in 7 out of 13 objects. Only five objects show both maser and continuum emission, and two objects were detected in neither line nor continuum. Figures 2–12 show a 1″ square field of view of the first moment maser maps and continuum contours and they show spectra of the detected objects (in line, continuum, or both). Table 2 lists the maser and continuum centroids based on two-dimensional Gaussian fits. For the spectral lines, these fits were made to the integrated line maps. The maser emission was universally unresolved, but the continuum emission was formally resolved when deconvolved from the beam in all but two objects, IC 485 and CGCG 168−018.

Table 2 also lists the maser-continuum offsets in angular and physical units. Offsets for four of the five objects detected in both maser and continuum are non-significant with 1σ uncertainties ranging from about 1 to 40 pc. The only object showing a significant offset between the maser and continuum centroids is CGCG 168−018, with a 21.6 ± 2.7 pc offset (Figure 11).

Table 3 lists the measured and derived water maser properties: peak and integrated flux densities, luminosity distance, isotropic line luminosity, the range of velocities spanned by the line emission 3σ above the noise, the velocity of peak emission, and the adopted systemic velocity. For J0804+3607, we list redshifts rather than velocities. The detected maser velocities are consistent with previous observations, although the masers can be substantially offset from the systemic velocities, which are obtained from optical and HI 21 cm lines. It is unclear whether these velocity offsets are physical (i.e., due to different line-emitting regions genuinely having different velocities, as is seen in shock-induced maser emission), due to obscuration (optical vs. radio lines), or due to measurement error, particularly in optical redshifts. We therefore do not rely on the velocity offset between the maser emission and the adopted systemic velocity as a criterion for assessing the likelihood of a maser arising from an inclined disk. Isotropic maser luminosities range from kilomaser values (3.05 ± 0.26 $L_\odot$ in NGC 520b) to the exceptionally luminous, $L_{iso} = (1.8 \pm 0.1) \times 10^4$ $L_\odot$ in J0804+3607 (Section 7).

Table 4 shows the 20 GHz radio continuum properties of the seven detected objects. We include the peak flux density, the integrated flux density, the spectral index derived solely from the 18–22 GHz bandpass, and the deconvolved angular size. Among the six continuum sources with enough signal-to-noise to derive a significant spectral index, four are steep spectrum ($\alpha = -1$ to -2) and two are flat ($\alpha \simeq -0.2 \pm 0.2$). One of the latter, CGCG 120−039, is only marginally resolved. IC 485, which does not have a spectral index measurement, but which shows both maser and continuum emission, does not have a resolved continuum.

6. ANALYSIS

Figure 13 shows the projected physical offset between the water maser line and continuum centroids for the five objects detected in both line and continuum (Table 2). Only CGCG 168−018 shows a significant offset of 29.3 ± 3.6 milliarcseconds or 21.6 ± 2.7 pc, but based on its 18–22 GHz continuum spectral index of $-0.95 \pm$

Table 1. Journal of Observations

Galaxy	UT Date	Integration	Beam[a]			Line		Continuum
			Angular	PA	Physical	rms	Δv	rms
		(m)	(milliarcsec)	(°)	(pc)	(mJy bm^{-1})	(km s^{-1})	(μJy bm^{-1})
NGC 291	2015-06-21	23.3	128 × 84	20.4	50 × 33	2.6	1.2	17
NGC 520b	2015-06-21	23.3	102 × 89	27.8	14 × 12	3.1	1.1	20
J0350−0127	2015-06-21	23.3	100 × 87	20.5	81 × 70	3.1	1.2	15
IC 485	2015-09-26	23.4	84 × 82	19.6	47 × 46	2.2	1.2	18
J0804+3607	2015-09-26	23.3	151 × 130	−81.3	1065 × 917	0.9	1.9	47
CGCG 120−039	2015-09-26	23.3	85 × 81	33.7	44 × 42	2.1	1.2	20
J0912+2304	2015-09-06	23.3	92 × 81	65.6	67 × 59	2.9	1.2	16
J1011−1926	2015-09-06	23.4	173 × 86	−20.8	98 × 49	5.3	1.2	19
NGC 3359[b]	2015-09-15	23.3	112 × 72	48.6	9 × 6	···	1.1	···
NGC 3556[b]	2015-09-15	23.3	104 × 72	45.0	6 × 4	···	1.1	···
NGC 3735[b]	2015-09-15	23.3	112 × 68	36.8	21 × 13	···	1.2	···
UGC 7016	2015-09-06	23.3	114 × 91	−74.8	54 × 43	3.8	1.2	16
NGC 5256	2015-06-19	23.3	96 × 84	−73.8	55 × 48	3.0	1.2	17
NGC 5691	2015-06-19	23.4	131 × 85	39.3	15 × 9	3.7	1.1	17
CGCG 168−018	2015-06-19	23.3	86 × 82	50.0	63 × 60	2.7	1.2	15
J1939−0124	2015-06-19	25.0	96 × 87	37.7	41 × 38	3.0	1.2	16

[a] Synthesized beam properties for the spectral line observations. The continuum maps are slightly different.

[b] Objects observed on 2015 September 15 could not be calibrated or imaged due to poor weather.

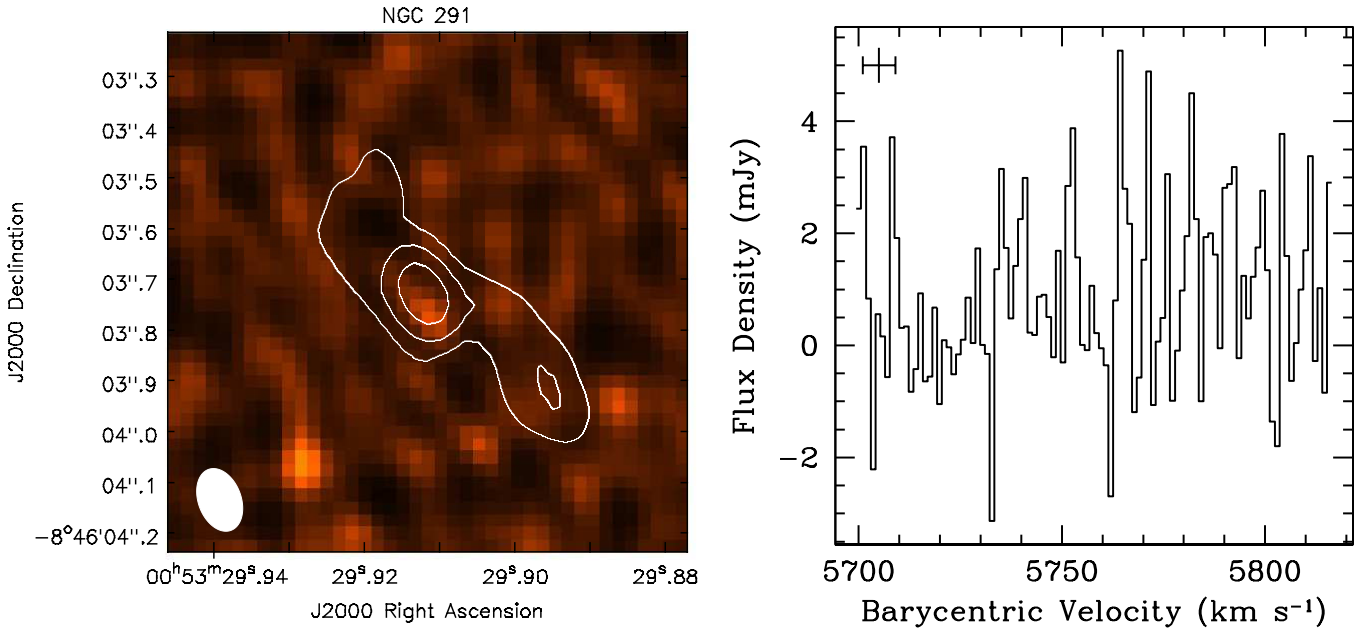

Figure 2. Left: NGC 291 integrated water maser (image) and 20 GHz radio continuum (contours) maps. Continuum contours indicate 4, 8, and 16 times the rms noise listed in Table 1. The spectral line beam is shown in the lower left (properties listed in Table 1). The 1″ field of view is equivalent to 393 pc. Right: water maser nondetection spectrum at the continuum peak with the systemic velocity and its uncertainty indicated by the vertical bars (5705 ± 4 km s^{-1}; Abazajian et al. 2004). The spectrum is roughly centered on the previous single-dish water maser detection (see Section 7).

Table 2. Maser and Radio Continuum Positions

Galaxy	Maser Centroid[a]		Continuum Centroid[b]		Offset	
	RA (hms)	Dec (dms)	RA (hms)	Dec (dms)	Angular (milliarcsec)	Physical (pc)
NGC 291	···	···	00:53:29.9101(11)	−08.46.03.740(14)	···	···
NGC 520b	01:24:34.91412(14)	+03.47.29.7864(22)	01:24:34.9099(28)	+03.47.29.7783(92)	64(42)	8.6(5.6)
J0350−0127	03:50:00.352168(29)	−01.27.57.39574(53)	···	···	···	···
IC 485	08:00:19.752486(74)	+26.42.05.0526(10)	08:00:19.7515(14)	+26.42.05.050(14)	13(19)	7.6(10.5)
J0804+3607	08:04:31.01144(40)	+36.07.18.1937(52)	08:04:31.01138(12)	+36.07.18.19927(91)	5.6(5.3)	39.6(37.2)
CGCG 120−039	08:49:14.07078(16)	+23.22.48.9408(20)	08:49:14.07097(13)	+23.22.48.9346(17)	6.7(2.7)	3.5(1.4)
J0912+2304	09:12:46.36659(33)	+23.04.27.2421(28)	···	···	···	···
J1011−1926	10:11:50.56731(17)	−19.26.43.9645(59)	···	···	···	···
UGC 7016	···	···	···	···	···	···
NGC 5256[c]	···	···	13:38:17.79219(15)	+48.16.41.1389(19)	···	···
	···	···	13:38:17.24843(76)	+48.16.32.2095(92)	···	···
NGC 5691	···	···	···	···	···	···
CGCG 168−018	16:30:40.90329(19)	+30.29.19.7066(29)	16:30:40.90134(21)	+30.29.19.7216(20)	29.3(3.6)	21.6(2.7)
J1939−0124	19:39:38.91545(38)	−01.24.33.2553(39)	···	···	···	···

[a] All detected maser emission was unresolved. See Table 1 for beam sizes.

[b] All detected continuum emission was resolved except for IC 485 and CGCG 168−018. See Table 4 for continuum measurements.

[c] NGC 5256 shows two widely-separated continuum components (both are listed).

NOTE—Coordinates are epoch J2000, and parenthetical values indicate uncertainties in the ultimate digits.

Table 3. Water Maser Properties and Redshifts

Galaxy	$S_{\rm peak}$[a] (mJy)	$S_{\rm int}$[b] (mJy km s^{-1})	D_L (Mpc)	$L_{\rm iso}$[c] ($L_\odot$)	$v_{\rm range}$[d] (km s^{-1})	$v_{\rm peak}$ (km s^{-1})	$v_{\rm sys}$ (km s^{-1})	Ref.[e]
NGC 520b	35(3)	166(14)	28	3.05(26)	2270–2273	2272(1)	2288(8)	1
J0350−0127	347(4)	7200(150)	180	5181(108)	12336–12393[f]	12369(1)	12322(18)	2
IC 485	78(2)	2470(130)	125	868(46)	8307–8387	8356(1)	8338(10)	3
J0804+3607[g]	9(1)	80(6)	3997	$1.8(1)\times10^4$	0.66038–0.66051	0.66045(1)	0.65654(37)	4
CGCG 120−039	82(2)	438(46)	116	133(14)	7559–7565	7565(1)	7684(26)	5
J0912+2304	16(3)	252(44)	164	151(26)	10855–10878	10855(1)	10861(26)	6
J1011−1926	44(4)	624(82)	123	213(28)	8043–8065	8048(1)	8065(31)	7
CGCG 168−018	25(2)	279(36)	162	163(21)	11134–11164	11140(1)	11015(29)	5
J1939−0124	30(2)	519(80)	93	102(16)	6170–6206	6198(1)	6226(20)	8

[a] The peak flux density was obtained from a spectrum formed from a single beam centered on the peak (unresolved) maser emission.

[b] The integrated flux density of the water maser complex was obtained from fitting a single two-dimensional Gaussian to the velocity-integrated spectral line cube.

[c] The isotropic luminosity is computed from the integrated line flux density S_{int} via $L_{iso} = 23.1\ L_\odot \times S_{\rm int}({\rm mJy\ km\ s^{-1}}) \times D_L({\rm Gpc})^2/(1+z)$, where D_L is the luminosity distance and z is the cosmological redshift.

[d] $v_{\rm range}$ is the velocity range over which the water maser exceeds 3σ significance.

[e] References for the systemic velocities: 1 – Springob et al. (2005); 2 – Huchra et al. (2012); 3 – de Vaucouleurs et al. (1991); 4 – Hewett & Wild (2010); 5 – Adelman-McCarthy et al. (2007); 6 – Adelman-McCarthy et al. (2008); 7 – Jones et al. (2009); 8 – Theureau et al. (2007).

[f] There appears to be an additional narrow maser line at 12422 km s^{-1} (Figure 4).

[g] We list redshifts instead of velocities for $v_{\rm range}$, $v_{\rm peak}$, and $v_{\rm sys}$ for J0804+3607.

NOTE—Only objects with detected water maser emission are listed (see Table 1 for rms noise values for nondetections). Parenthetical values indicate uncertainties in the ultimate digits.

0.17 (Table 4), the continuum could be jet emission and not the core of the AGN. All other maser-continuum offsets are not significant and are therefore consistent with inclined maser disk expectations.

7. DISCUSSION

Among the 13 water maser hosts, we did not detect water masers in four objects: NGC 291, UGC 7016, NGC 5256, and NGC 5691. The water maser in NGC 520b is likely associated with star formation and is rejected as an inclined maser disk candidate (see 7.1.2). Objects with unresolved masers but not detected in the 20 GHz continuum remain ambiguous (these are J0350−0127, J0912+2304, J1011−1926, and J1939−0124; note that none of these have other sub-arcsecond radio continuum observations), as does CGCG 168−018, the only object to show a significant maser-continuum offset (see 7.1.12). IC 485, J0804+3607, and CGCG 120−039 remain inclined maser disk candidates: they show no significant maser-continuum offset and no high velocity lines (by selection). While the maser emission from IC 485 is broad and multi-component, this type of structure spanning ∼100 km s^{-1} is seen in the systemic masers in many disk systems (e.g., Kuo et al. 2011). J0808+3607 and CGCG 120−039 have narrow maser lines and are particularly good inclined disk candidates.

7.1. *Individual Objects*

We discuss the previous water maser observations, general characteristics, and our results for each individual object below.

7.1.1. *NGC 291*

NGC 291 is a barred spiral galaxy with a Seyfert 2 nucleus (Kewley et al. 2001; Nair & Abraham 2010). The maser was detected as a narrow ∼60 mJy line in 2006 by GBT program GBT06A-009,[2] but we did not detect it (2.6 mJy beam^{-1} rms per 1.2 km s^{-1} channel; Table 1 and Figure 2) nor did Kondratko et al. (2006) in 2002 (15 mJy rms per 1.3 km s^{-1} channel). We detect extended 20 GHz continuum with 18–22 GHz spectral index -2.0 ± 0.3 (Table 4).

7.1.2. *NGC 520b*

Table 4. 20 GHz Radio Continuum Properties

Galaxy	$S_{\rm peak}$[a]	$S_{\rm int}$[a]	α[b]	Size[a]		
				Angular	PA	Physical
	(μJy bm^{-1})	(mJy)		(milliarcsec)	(°)	(pc)
NGC 291	263(24)	1.93(20)	−2.0(3)	451(52) × 146(19)	51.8(3.4)	177(20) × 57(7)
NGC 520b	272(31)	4.31(52)	−0.23(19)	775(100) × 164(24)	95.6(2.3)	105(14) × 22(3)
IC 485	77(15)	0.180(48)	···	< 93 × 88	−69.5	< 52 × 49
J0804+3607	4247(83)	4.71(16)	−1.5(3)	62(12) × 23(13)	71(17)	437(85) × 162(92)
CGCG 120−039	482(20)	0.555(39)	−0.27(16)	44(8) × 23(14)	133(33)	23(4) × 12(7)
NGC 5256[c]	633(28)	1.543(68)	−2.0(2)	127(6) × 96(8)	148.7(9.6)	72(3) × 55(5)
	78(17)	0.48(11)	···	433(23) × 68(58)	163.1(3.1)	247(13) × 39(33)
CGCG 168−018	267(16)	0.308(30)	−0.95(17)	< 87 × 85	77.8	< 64 × 63

[a] The peak flux density, integrated flux density, and the radio source size and orientation were obtained from fitting a single two-dimensional Gaussian to the source image and deconvolving the source from the beam. Upper limits indicate unresolved detections and list the continuum beam parameters.

[b] The spectral index α was measured at the peak of the continuum emission solely from within the 18–22 GHz bandpass and follows the convention $S_\nu \propto \nu^\alpha$. It is not listed for objects with inadequate signal-to-noise in the 20 GHz continuum.

[c] NGC 5256 shows two widely-separated continuum components (both are listed).

NOTE—Only objects with detected 20 GHz continuum emission are listed (see Table 1 for rms noise values for nondetections). Parenthetical values indicate uncertainties in the ultimate digits.

NGC 520b is one galaxy in the colliding pair in NGC 520 (e.g., Stanford & Balcells 1990). Castangia et al. (2008) detected a maser in 2005, measuring a ∼ 40 mJy peak with the VLA and $L_{iso} \sim 1\ L_\odot$. Our VLA detection shows a 35 ± 3 mJy peak and $L_{iso} = 3.05 \pm 0.26\ L_\odot$ (Figure 3 and Table 3). Our VLA map shows extended 20 GHz radio continuum emission (Figure 3, bottom) with a flat 18–22 GHz spectral index of -0.23 ± 0.19 (Table 4) and a similar east-west morphology to the Castangia et al. (2008) 14.9 GHz map. In our map the maser is slightly north of the Castangia et al. (2008) maser position. There is a significant maser-continuum peak offset, although the single-component centroid fits listed in Table 2 are consistent because the radio emission is extended. Castangia et al. (2008) favor a star formation origin for the water maser in NGC 520b, but cannot rule out a low luminosity AGN. The preponderance of evidence suggests that NGC 520b is a poor candidate for an inclined maser disk.

7.1.3. *J0350−0127*

J0350−0127 is an almost otherwise unknown spiral or possibly irregular galaxy included in the 2MASS Redshift Survey (Huchra et al. 2012) and detected in water maser emission by the GBT programs GBT09-051[2] in 2010 and GBT10C-019[2] in 2011. The peak flux density was ∼350 mJy in 2011, in good agreement with our VLA measurement of 347 ± 4 mJy (Table 3 and Figure 4). This is a broad and luminous maser ($L_{\rm iso} = 5181 \pm 108\ L_\odot$) with no associated 20 GHz continuum, down to an rms noise of 15 μJy beam^{-1} (Table 1). Without a continuum detection, the nature of this maser remains ambiguous, although it is almost certainly associated with an AGN.

7.1.4. *IC 485*

IC 485 is a spiral galaxy detected in the water maser line in 2006 in GBT program GBT06C-035.[2] The maser has a ∼80 mJy peak and shows a broad profile. Zhu et al. (2011) lists this object as a maser nondetection. Our VLA observations show a broad, multi-component maser with a similar peak (78 ± 2 mJy) and a high luminosity, $L_{iso} = 868 \pm 46\ L_\odot$ (Figure 5 and Table 3). The 20 GHz continuum is detected but unresolved and faint (77 ± 15 μJy beam^{-1} peak flux density; Table 4). This galaxy was also detected at 1.4 GHz (4.4 mJy), and its dominant radio energy source was classified as star formation by Condon et al. (2002). This classification does not exclude the presence of an AGN: Liu et al. (2011) classify the optical nucleus of IC 485 as a LINER. The maser-continuum offset is not significant — less than 10.5 pc (1σ; Table 2) — so this maser remains an inclined disk candidate.

7.1.5. *J0804+3607*

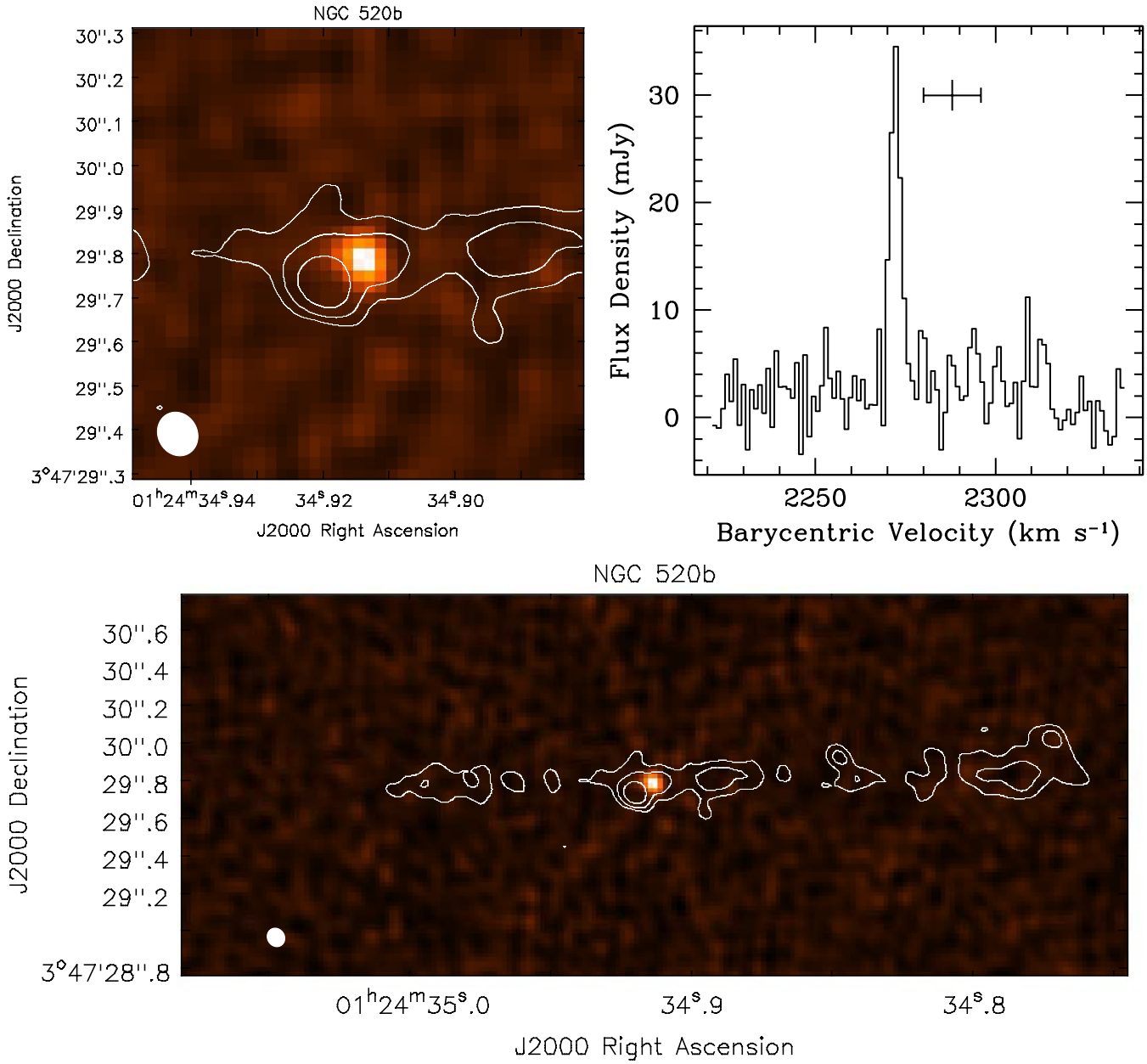

Figure 3. Top Left: NGC 520b integrated water maser (image) and 20 GHz radio continuum (contours) maps. Continuum contours indicate 4, 8, and 16 times the rms noise listed in Table 1. The spectral line beam is shown in the lower left (properties listed in Table 1). The 1″ field of view is equivalent to 135 pc. Top Right: water maser spectrum with the systemic velocity and its uncertainty indicated by the vertical bars (Table 3). The spectrum is roughly centered on the previous single-dish water maser detection (see Section 7). Bottom: a 5″×2″ (675 pc × 170 pc) field of view to show the full extent of the 20 GHz continuum.

This is a type 2 quasar showing luminous water maser emission at $z \simeq 0.66$ (Zakamska et al. 2003; Barvainis & Antonucci 2005). The isotropic maser luminosity was $2.31 \pm 0.46 \times 10^4$ $L_\odot$ in 2005 (Barvainis & Antonucci 2005, error from the quoted 20% calibration uncertainty) and $1.8 \pm 0.1 \times 10^4$ $L_\odot$ in 2015 (this work), consistent with no variation. The maser and 20 GHz continuum emission are coincident to within 40 pc (1σ; Table 2 and Figure 6), which is less precise than the other objects due to the much larger distance and lower observing frequency. The 12–16 GHz spectral index is -1.5 ± 0.3 (Table 4). This object remains an inclined maser disk candidate.

7.1.6. *CGCG 120−039*

The water maser in this little-studied galaxy was detected in 2013 in GBT program GBT13A-236.[2] It had a peak flux density of ∼210 mJy, was blueshifted from the systemic velocity, and showed several components.

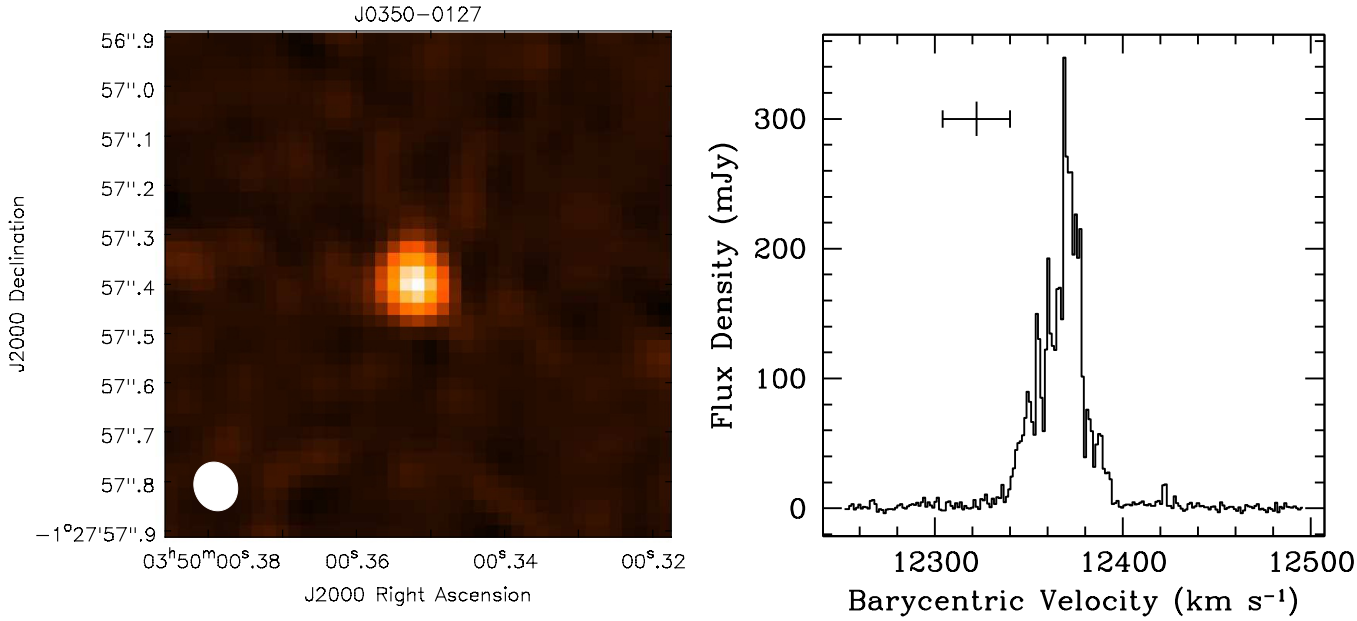

Figure 4. Left: J0350−0127 integrated water maser map. The 20 GHz continuum was not significantly detected. The spectral line beam is shown in the lower left (properties listed in Table 1). The 1″ field of view is equivalent to 805 pc. Right: water maser spectrum with the systemic velocity and its uncertainty indicated by the vertical bars (Table 3). The spectrum is roughly centered on the previous single-dish water maser detection (see Section 7).

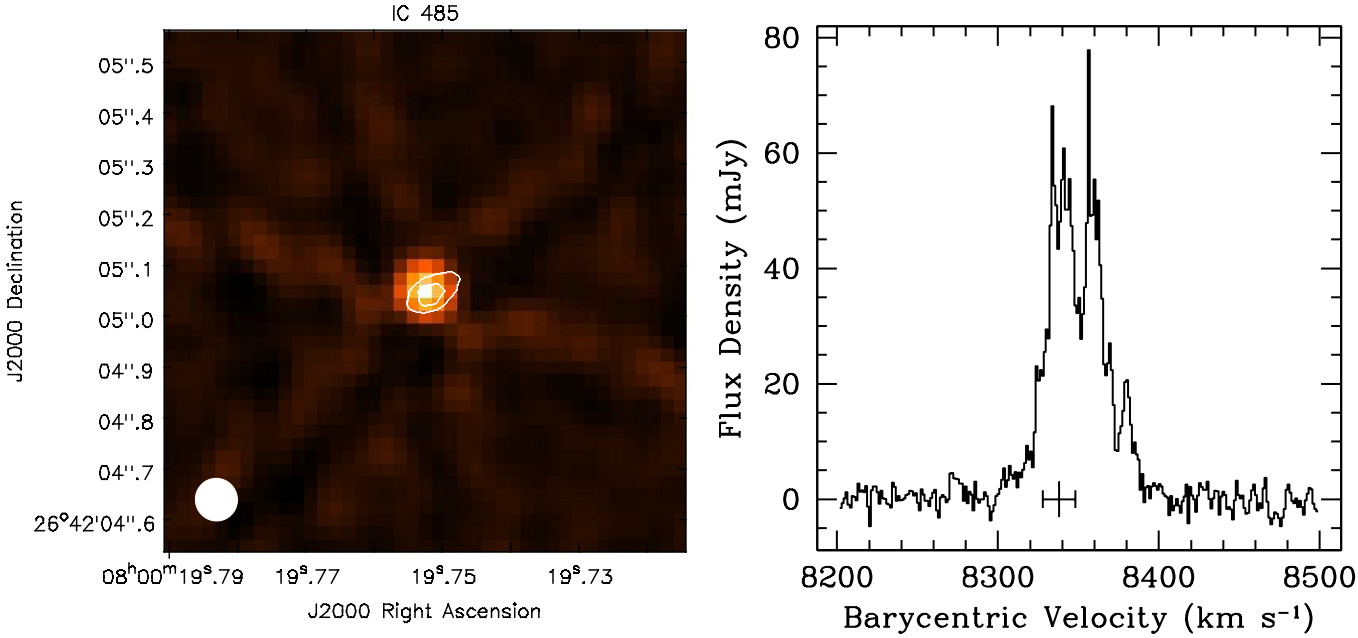

Figure 5. Left: IC 485 integrated water maser (image) and 20 GHz radio continuum (contours) maps. Continuum contours indicate 3 and 4 times the rms noise listed in Table 1. The spectral line beam is shown in the lower left (properties listed in Table 1). The 1″ field of view is equivalent to 562 pc. Right: water maser spectrum with the systemic velocity and its uncertainty indicated by the vertical bars (Table 3). The spectrum is centered on the previous single-dish water maser detection (see Section 7).

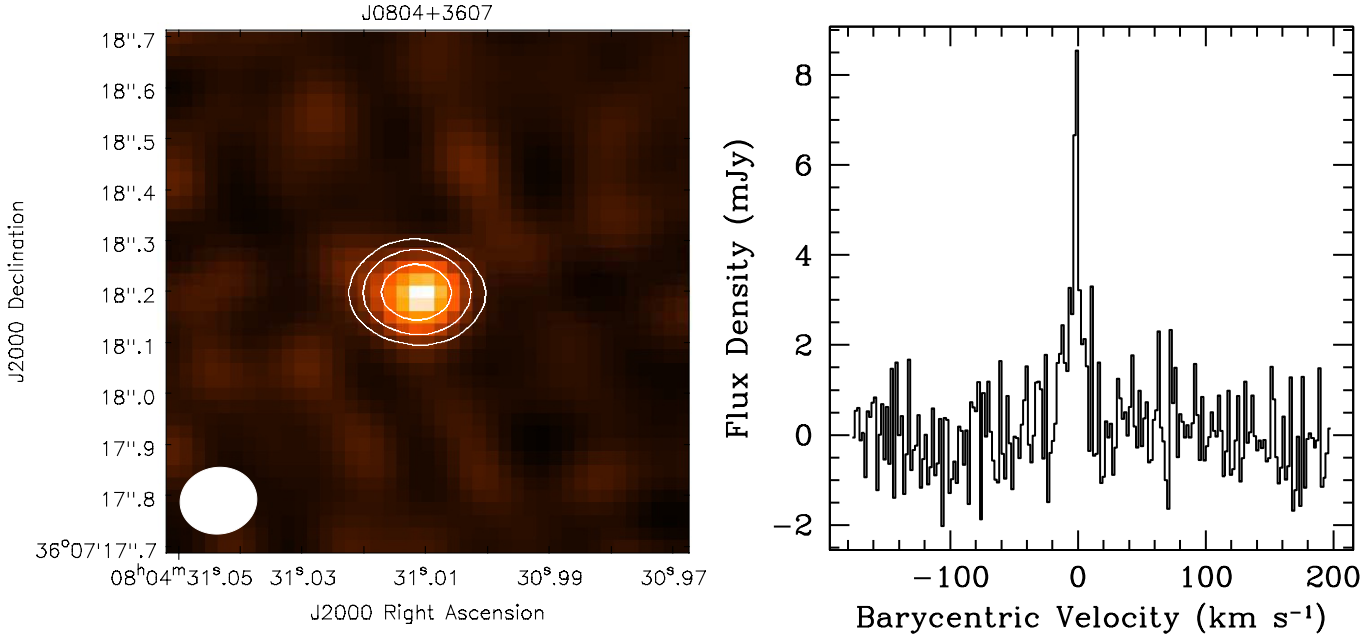

Figure 6. Left: J0804+3607 integrated water maser (image) and 14 GHz radio continuum (contours) maps. Continuum contours indicate 4, 8, and 16 times the rms noise listed in Table 1. The spectral line beam is shown in the lower left (properties listed in Table 1). The 1″ field of view is equivalent to 7.055 kpc. Right: water maser spectrum centered on the peak maser emission at $z = 0.66045$, plotted in the object rest frame (Table 3).

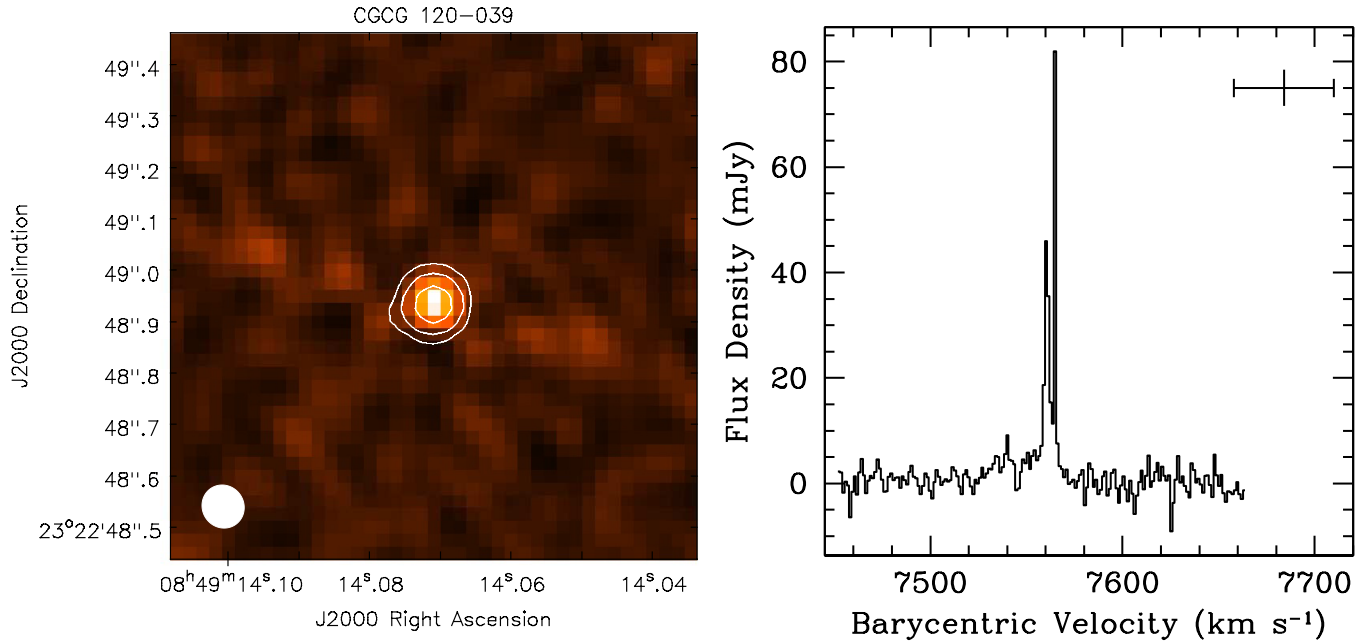

Figure 7. Left: CGCG 120−039 integrated water maser (image) and 20 GHz radio continuum (contours) maps. Continuum contours indicate 4, 8, and 16 times the rms noise listed in Table 1. The spectral line beam is shown in the lower left (properties listed in Table 1). The 1″ field of view is equivalent to 519 pc. Right: water maser spectrum with the systemic velocity and its uncertainty indicated by the vertical bars (Table 3). The spectrum is roughly centered on the previous single-dish water maser detection (see Section 7).

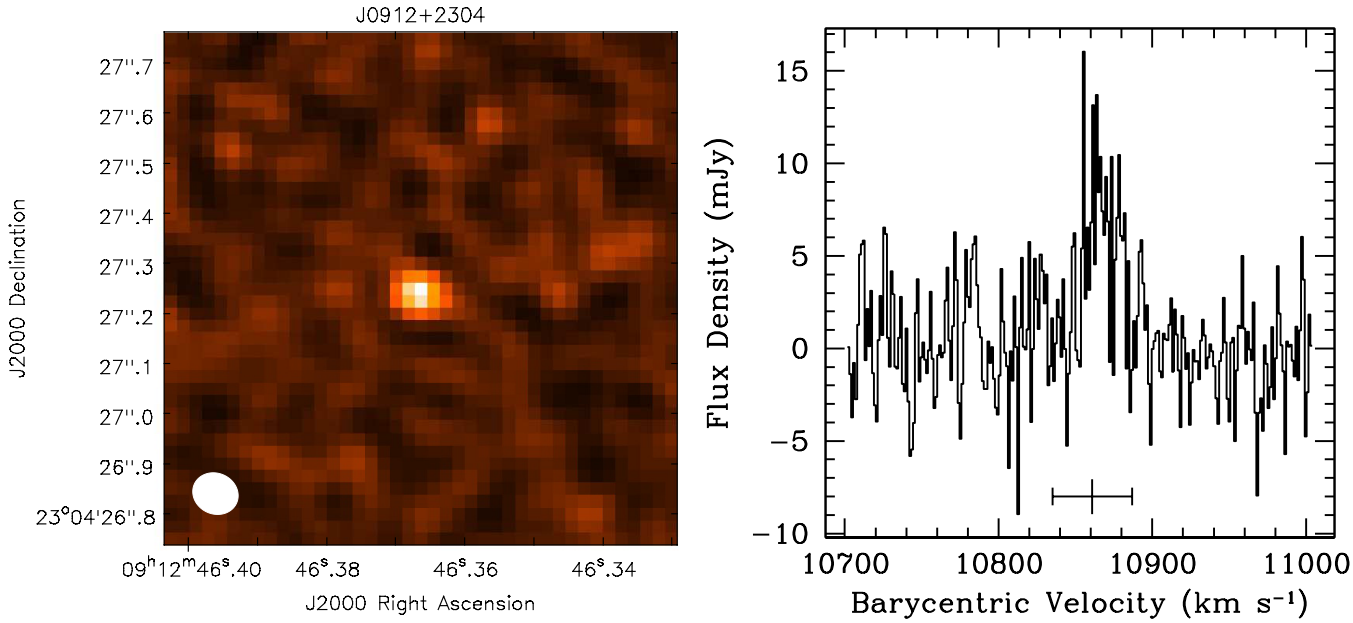

Figure 8. Left: J0912+2304 integrated water maser map. The 20 GHz continuum was not significantly detected. The spectral line beam is shown in the lower left (properties listed in Table 1). The 1″ field of view is equivalent to 723 pc. Right: water maser spectrum with the systemic velocity and its uncertainty indicated by the vertical bars (Table 3). The spectrum is centered on the previous single-dish water maser detection (see Section 7).

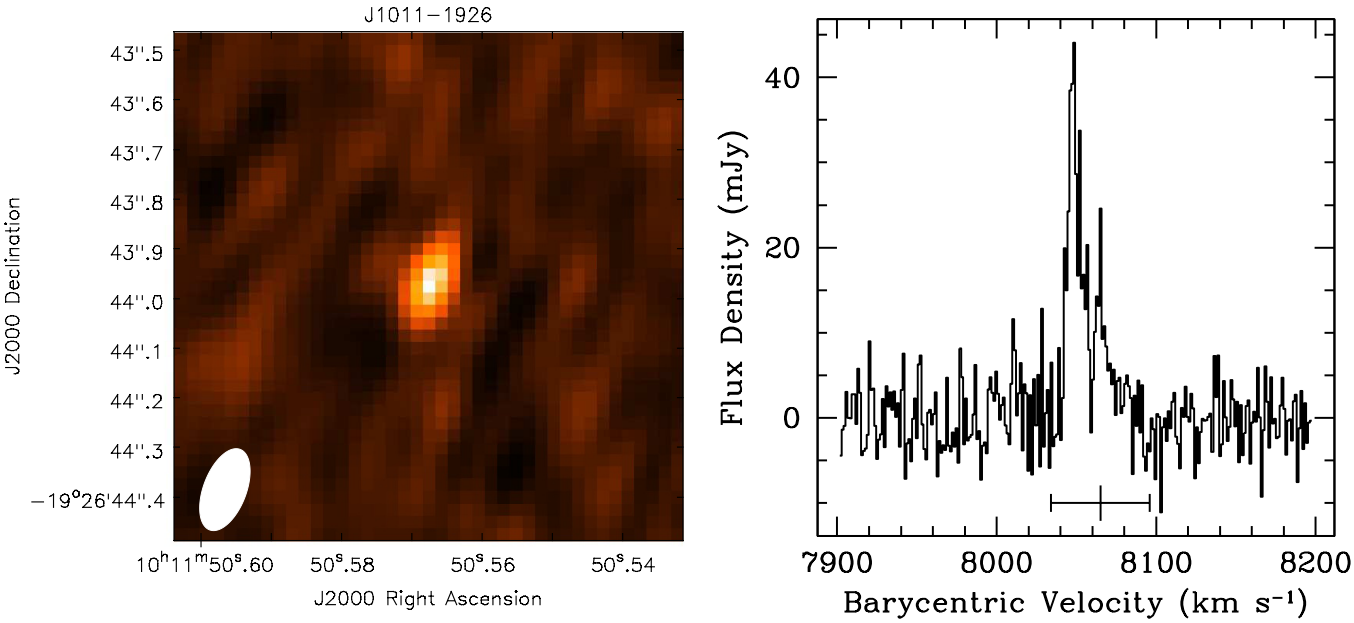

Figure 9. Left: J1011−1926 integrated water maser map. The 20 GHz continuum was not significantly detected. The spectral line beam is shown in the lower left (properties listed in Table 1). The 1″ field of view is equivalent to 564 pc. Right: water maser spectrum with the systemic velocity and its uncertainty indicated by the vertical bars (Table 3). The spectrum is centered on the previous single-dish water maser detection (see Section 7).

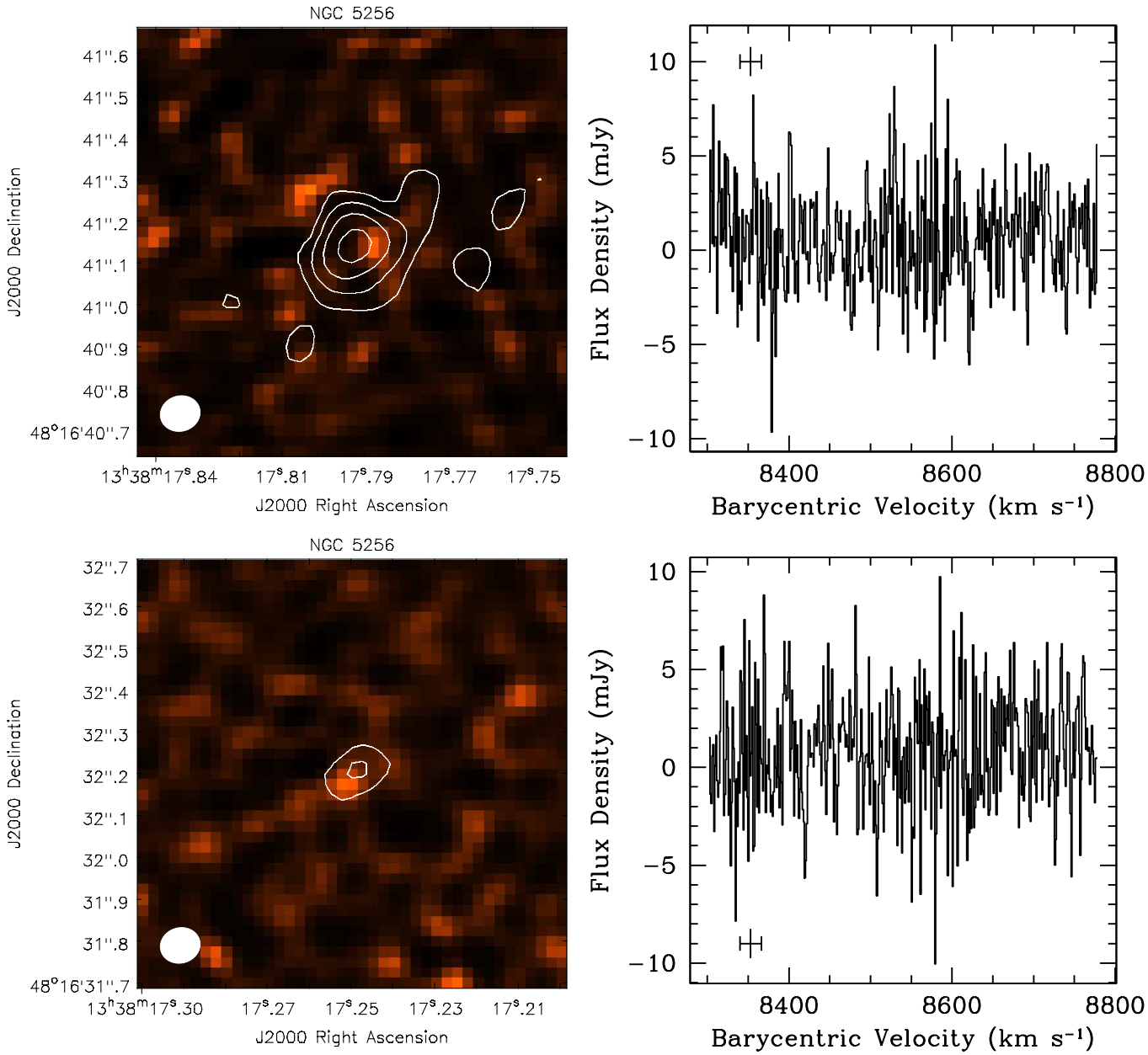

Figure 10. Left: NGC 5256 integrated water maser (image) and 20 GHz radio continuum (contours) maps. Continuum contours indicate 4, 8, 16, and 32 times the rms noise listed in Table 1. The spectral line beam is shown in the lower left (properties listed in Table 1). The 1″ field of view is equivalent to 570 pc. Right: water maser nondetection spectra at the continuum peaks with the systemic velocity and its uncertainty indicated by the vertical bars (8353 ± 13 km s^{-1}; de Vaucouleurs et al. 1991). The spectra are roughly centered on the previous single-dish water maser detection (see Section 7). Two continuum sources were detected, but no water maser emission was detected toward either continuum source or in the larger field of view.

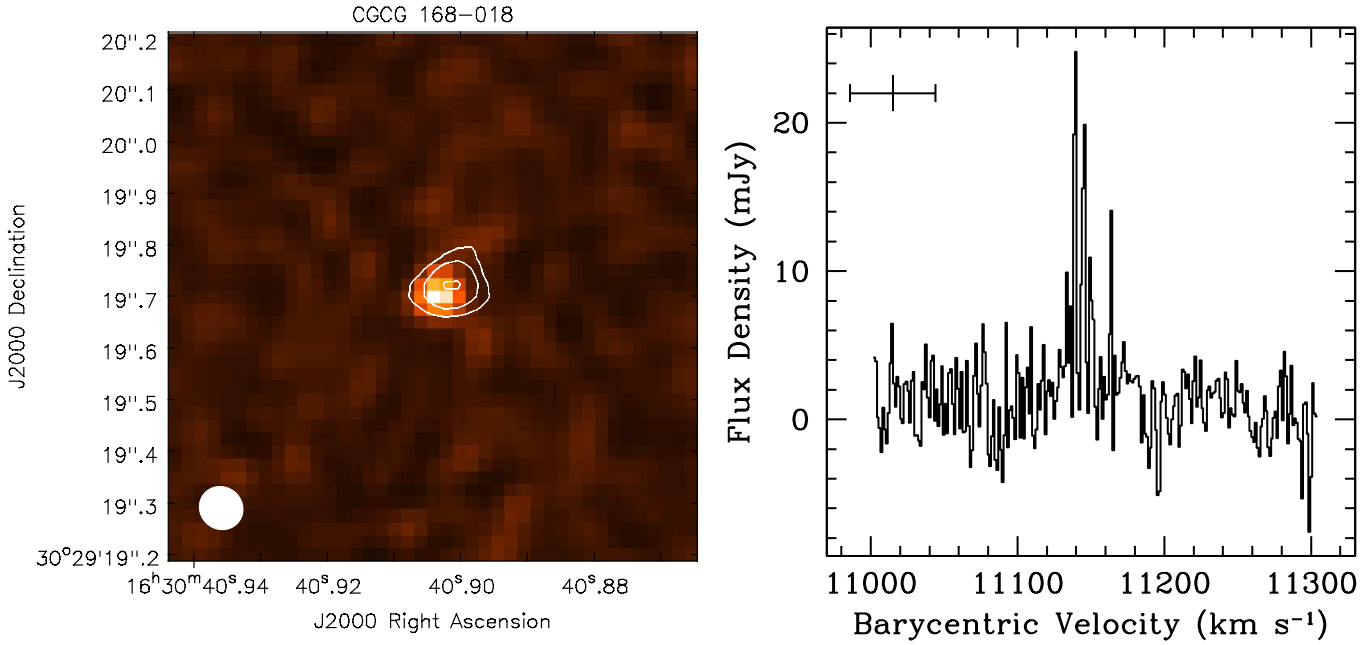

Figure 11. Left: CGCG 168−018 integrated water maser (image) and 20 GHz radio continuum (contours) maps. Continuum contours indicate 4, 8, and 16 times the rms noise listed in Table 1. The spectral line beam is shown in the lower left (properties listed in Table 1). The 1″ field of view is equivalent to 737 pc. Right: water maser spectrum with the systemic velocity and its uncertainty indicated by the vertical bars (Table 3). The spectrum is roughly centered on the previous single-dish water maser detection (see Section 7).

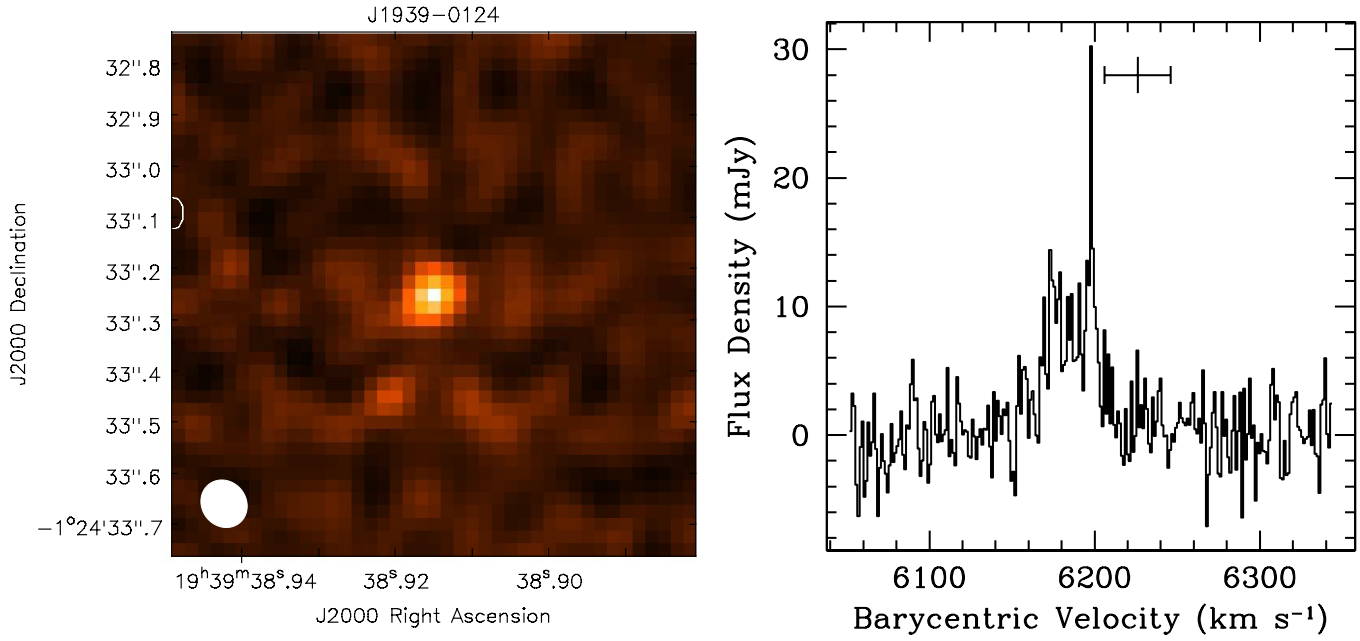

Figure 12. Left: J1939−0124 integrated water maser map. The 20 GHz continuum was not significantly detected. The spectral line beam is shown in the lower left (properties listed in Table 1). The 1″ field of view is equivalent to 432 pc. Right: water maser spectrum with the systemic velocity and its uncertainty indicated by the vertical bars (Table 3). The spectrum is roughly centered on the previous single-dish water maser detection (see Section 7).

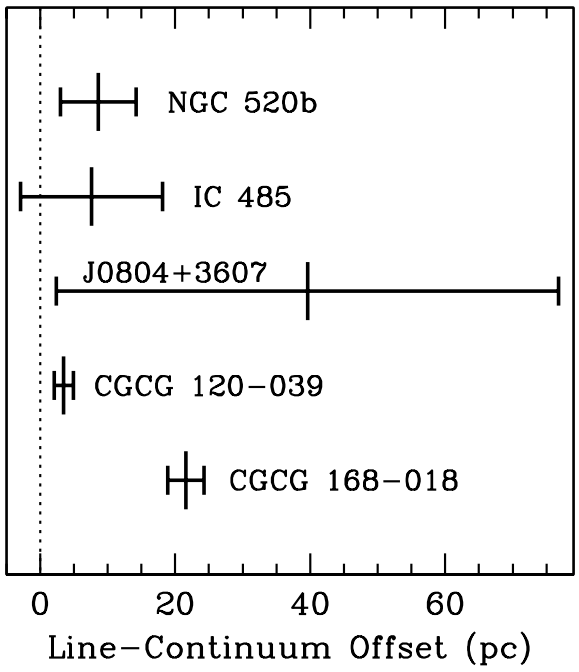

Figure 13. Maser-continuum offsets for those objects detected in both. Only CGCG 168−018 shows a significant offset. Error bars are plotted symmetrically.

We detect the maser — now at 82 ± 2 mJy peak, but still showing multiple components (Figure 7) — and the 20 GHz continuum at 0.56 ± 0.04 mJy, which are spatially coincident to within a remarkably small 3.5 ± 1.4 pc (Table 2). The 18–22 GHz spectral index is flat: $\alpha = -0.27 \pm 0.16$ (Table 4). This object is a good inclined maser disk candidate.

7.1.7. *J0912+2304*

The water maser in the galaxy J0912+2304 was detected in 2008 by GBT program GBT07A-034,[2] showing a ∼30 mJy peak. Zhu et al. (2011) list this as a water maser nondetection. The VLA observations show a 16 ± 3 mJy peak, but no 20 GHz continuum down to an rms noise of 16 μJy beam^{-1} (Figure 8 and Tables 1 and 3). The provenance of the maser remains ambiguous.

7.1.8. *J1011−1926*

The maser in this almost unknown galaxy was detected in GBT program GBT07A-066[2] in 2008. (Zhu et al. 2011) list this object as a water maser nondetection. The GBT detection shows a broad line with a ∼80 mJy peak. The VLA detection shows a broad multi-component maser with a 44 ± 4 mJy peak in good agreement with the systemic velocity (Figure 9 and Table 3). We do not detect the 20 GHz continuum. The nature of this maser therefore remains ambiguous.

7.1.9. *UGC 7016*

The water maser in this barred spiral (de Vaucouleurs et al. 1991) was detected in 2007 by GBT program GBT07A-034,[2] but Zhu et al. (2011) list this as a nondetection. The GBT detection spectrum had a peak flux density of ∼55 mJy, but we did not detect the maser or the 20 GHz continuum emission. VLA rms noise values were 3.8 mJy beam^{-1} per 1.2 km s^{-1} channel in the spectral line cube and 16 μJy beam^{-1} in the continuum map (Table 1).

7.1.10. *NGC 5256*

Braatz et al. (2004) discovered the water maser in this merging luminous infrared galaxy in 2003. It had a peak flux density of 99 mJy ($L_{iso} = 30\ L_{\odot}$) and was redshifted from the systemic velocity by ∼300 km s^{-1}. Braatz et al. (2004) claim that all maser emission originates from the southern nucleus (a Sey 2 nucleus according to, e.g., Mazzarella & Boroson 1993). We detect two 20 GHz continuum sources that are consistent with the positions of the two nuclei (Tables 2 and 4; Brown et al. 2014), but neither location (nor the larger region that includes the overlap region between the two nuclei) shows maser emission down to an rms noise of 3.0 mJy beam^{-1} in 1.2 km s^{-1} channels (Table 1 and Figure 10). The spectral index of the northern nuclear continuum is -2.0 ± 0.2 in the 18–22 GHz band (Table 4).

7.1.11. *NGC 5691*

The water maser in NGC 5691, a barred non-Seyfert spiral galaxy (Mulchaey et al. 1997), was detected in 2009 by GBT program AGBT08C-035[2] with a ∼45 mJy peak flux density. It was listed by Zhu et al. (2011) as a maser nondetection. We did not detect the maser or any 20 GHz continuum in this galaxy, with rms noise levels of 3.7 mJy beam^{-1} per 1.1 km s^{-1} channel and 17 μJy beam^{-1}, respectively (Table 1).

7.1.12. *CGCG 168−018*

CGCG 168−018 is a little-studied galaxy classified as an AGN by Schawinski et al. (2010) and listed as a water maser nondetection by Zhu et al. (2011). Water maser emission was detected by GBT program GBT07A-066[2] in 2008. The GBT water maser spectrum shows a ∼50 mJy peak, detected by this work at 25 ± 2 mJy (Table 3). The 0.31 ± 0.03 mJy continuum shows a 18-22 GHz spectral index of -0.95 ± 0.17 (Table 4). The maser emission and 20 GHz continuum are unresolved but show a significant relative offset of 21.6 ± 2.7 pc (Table 2 and Figure 11). This is the only object in the sample that shows a significant offset between the maser and continuum emission (Figure 13). While the offset suggests that the maser emission is not deflected from an inclined maser disk, the continuum spectral index suggests that

the continuum may arise from a jet, and the radio core is not detected. The provenance of the maser therefore remains ambiguous.

7.1.13. *J1939−0124*

Greenhill et al. (2003) detected the water maser in this spiral galaxy hosting a Sey 2 nucleus in 2002 using the Tidbinbilla antenna. The maser showed a peak flux density of ∼28 mJy, and Henkel et al. (2005) report $L_{iso} \simeq 160\ L_{\odot}$. No 22 GHz continuum was detected by Greenhill et al. (2003) using the VLA (< 2.8 mJy). We likewise detect no continuum, with rms noise of 16 μJy beam^{-1} (Table 1), but we do detect the maser emission with peak 30 ± 2 mJy ($L_{iso} = 102 \pm 16\ L_{\odot}$) although with a substantially different maser profile (Figure 12 and Table 3). The 6 and 20 cm continua were detected at 5.4 ± 0.4 mJy and 15.5 ± 1.0 mJy, respectively, by Vader et al. (1993), and the 6 cm continuum position agrees with the maser position to within ∼1″(∼430 pc). The nature of this maser remains ambiguous.

8. CONCLUSIONS

This paper presents a physical mechanism that may enable detection of inclined water maser disks orbiting massive black holes via the lensing/deflection of in-going systemic masers. The observational signature of an inclined disk is a maser line or line complex with limited Doppler extent that appears to arise at the location of the black hole, as identified by its radio continuum core. With enough angular resolution, it may be possible to measure the black hole mass if the maser emission forms a lensing arc or Einstein ring, but the mass precision will be limited by one's ability to measure or estimate the size of the maser-emitting portion of the disk.

We suggest that if inclined maser disks can be detected at all, then they have probably already been detected in single-dish surveys but discarded for interferometric follow-up because they did not show high-velocity lines. We present original 0.07–0.17″ (4–100 pc) resolution VLA observations of inclined maser disk candidates with the goal of identifying systems where the maser emission is unresolved and is coincident with the 20 GHz continuum emission.

Of the 16 masers observed with the VLA, we obtained useful data for 13, and among these, five were detected in both 22 GHz maser line emission and in 20 GHz continuum. Of these five, one maser is most likely associated with star formation (NGC 520b), and one shows a significant spatial offset between the maser emission and the continuum (CGCG 168−018, but it could still host an inclined maser disk — this case is ambiguous). Three objects are good inclined maser disk candidates that merit further study with VLBI: IC 485, J0804+3607, and CGCG 120−039. Five maser hosts remain ambiguous, based either on non-detected or offset continua: J0350−0127, J0912+2304, J1011−1926, CGCG 168−018, and J1939−0124.

More straightforward methods for measuring black hole masses from molecular lines may be in the offing. For example, Davis et al. (2013) and Barth et al. (2016a,b) have used carbon monoxide kinematics in thin disks that approach or are within the black hole gravitational sphere of influence to obtain black hole mass measurements. Barth et al. (2016a), in particular, demonstrate the ability of ALMA to measure black hole masses with ∼10% uncertainty. Although they lack the intrinsic brightness of masers that enables VLBI mapping, thermal molecular lines have the advantage of being observable at any disk inclination.

We thank A. Hamilton and M. Eracleous for helpful discussion and B. Butler for assistance with metadata repair of bespoke observing configurations. We also thank the anonymous referee for important feedback. This research has made use of NASA's Astrophysics Data System Bibliographic Services and the NASA/IPAC Extragalactic Database (NED), which is operated by the Jet Propulsion Laboratory, California Institute of Technology, under contract with the National Aeronautics and Space Administration.

Facility: VLA

Software: CASA

REFERENCES

Abazajian, K., Adelman-McCarthy, J. K., Agüeros, M. A., et al. 2004, AJ, 128, 502

Adelman-McCarthy, J. K., Agüeros, M. A., Allam, S. S., et al. 2007, ApJS, 172, 634

Adelman-McCarthy, J. K., Agüeros, M. A., Allam, S. S., et al. 2008, ApJS, 175, 297

Amiri, N., & Darling, J. 2016, ApJ, 826, 136

Argon, A. L., Greenhill, L. J., Reid, M. J., Moran, J. M., & Humphreys, E. M. L. 2007, ApJ, 659, 1040

Barth, A. J.; Boizelle, B. D., Darling, J., Baker, A. J., Buote, D. A., Ho, L. C., & Walsh, J. L. 2016, ApJL, 822, L28

Barth, A. J., Darling, J., Baker, A. J., Boizelle, B. D., Buote, D. A., Ho, L. C., & Walsh, J. L. 2016, ApJ, 823, 51

Barvainis, R. & Antonucci, R. 2005, ApJ, 628, L89

van den Bosch, R. C. E., Greene, J. E., Braatz, J. A., Constantin, A., & Kuo, C.-Y. 2016, ApJ, 819, 11

Braatz, J. A., Henkel, C., Greenhill, L. J., Moran, J. M., & Wilson, A. S. 2004, ApJ, 617, L29

Braatz, J. A., Reid, M. J., Humphreys, E. M. L., Henkel, C., Condon, J. J., & Lo, K. Y. 2010, ApJ, 718, 657

Brogan, C., Johnson, K., & Darling, J. 2010, ApJ, 716, L51

Brown, M. J. I., Moustakas, J., Smith, J.-D. T., da Cunha, E., Jarrett, T. H., Imanishi, M., Armus, L., Brandl, B. R., & Peek, J. E. G. 2014, ApJS, 212, 18
Castangia, P., Tarchi, A., Henkel, C., & Menten, K. M. 2008, A&A, 479, 111
Claussen, M. J., Diamond, P. J., Braatz, J. A., Wilson, A. S., & Henkel, C. 1998, ApJ, 500, L129
Condon, J. J., Cotton, W. D., & Broderick, J. J. 2002, AJ, 124, 675
Darling, J., Brogan, C., & Johnson, K. 2008, ApJ, 685, L39
Darling, J. 2011, ApJ, 732, L2
Davis, T. A., Bureau, M., Cappellari, M., Sarzi, M., & Blitz, L. 2013, Nature, 494, 328
Einstein, A. 1915, Preussische Akademie der Wissenschaften, Sitzungsberichte, (part 2), 831
Einstein, A. 1936, Science, 84, 506
Gallimore, J. F., Baum, S. A., O'Dea, C. P., Brinks, E., & Pedlar, A. 1996, ApJ, 462, 740
Gao, F., Braatz, J. A., Reid, M. J., Lo, K. Y., Condon, J. J., Henkel, C., Kuo, C. Y., Impellizzeri, C. M. V., Pesce, D. W., & Zhao, W. 2016, ApJ, 817, 128
Greene, J. E., Seth, A., Kim, M., Läsker, R., Goulding, A. D., Gao, F., Braatz, J. A., Henkel, C., Condon, J., Lo, F. K. Y., & Zhao, W. 2016, in press, (arXiv:1606.00018)
Greenhill, L. J., Henkel, C., Becker, R., Wilson, T. L., & Wouterloot, J. G. A. 1995, A&A, 304, 21
Greenhill, L. J., Herrnstein, J. R., Moran, J. M., Menten, K. M., & Velusamy, T. 1997, ApJ, 486, L15
Greenhill, L. J., Kondratko, P. T., Lovell, J. E. J., Kuiper, T. B. H., Moran, J. M., Jauncey, D. L., & Baines, G. P. 2003, ApJ, 582, L11
Greenhill, L. J., Booth, R. S., Ellingsen, S. P., Herrnstein, J. R., Jauncey, D. L., McCulloch, P. M., Moran, J. M., Norris, R. P., Reynolds, J. E., & Tzioumis, A. K. 2003, ApJ, 590, 162
Henkel, C., Peck, A. B., Tarchi, A., Nagar, N. M., Braatz, J. A., Castangia, P., & Moscadelli, L. 2005, A&A, 436, 75
Herrnstein, J. R., Greenhill, L. J., Moran, J. M., Diamond, P. J., Inoue, M., Nakai, N., & Miyoshi, M. 1998, ApJ, 497, L69
Hewett, P. C. & Wild, V. 2010, MNRAS, 405, 2302
Hofner, P., Baan, W. A., & Takano, S. 2006, AJ, 131, 2074
Huchra, J. P., Macri, L. M., Masters, K. L., et al. 2012, ApJS, 199, 26
Humphreys, E. M. L., Reid, M. J., Moran, J. M., Greenhill, L. J., & Argon, A. L. 2013, ApJ, 775, 13
Jones, D. H., Read, M. A., Saunders, W., et al. 2009, MNRAS, 399, 683
Kewley, L. J., Heisler, C. A., Dopita, M. A., & Lumsden, S. 2001, ApJS, 132, 37
Kondratko, P. T., Greenhill, L. J., & Moran, J. M. 2005, ApJ, 618, 618
Kondratko, P. T., Greenhill, L. J., Moran, J. M., et al. 2006, ApJ, 638, 100
Kuo, C. Y., Braatz, J. A., Condon, J. J., Impellizzeri, C. M. V., Lo, K. Y., Zaw, I., Schenker, M., Henkel, C., Reid, M. J., & Greene, J. E. 2011, ApJ, 727, 20
Kuo, C. Y., Braatz, J. A., Lo, K. Y., Reid, M. J., Suyu, S. H., Pesce, D. W., Condon, J. J., Henkel, C., & Impellizzeri, C. M. V. 2015, ApJ, 800, 26
Liu, X., Shen, Y., Strauss, M. A., & Hao, L. 2011, ApJ, 737, 101
Mazzarella, J. M. & Boroson, T. A. 1993, ApJS, 85, 27
McMullin, J. P., Waters, B., Schiebel, D., Young, W., & Golap, K. 2007, Astronomical Data Analysis Software and Systems XVI (ASP Conf. Ser. 376), ed. R. A. Shaw, F. Hill, & D. J. Bell (San Francisco, CA: ASP), 127
Miyoshi, M., Moran, J., Herrnstein, J., Greenhill, L., Nakai, N., Diamond, P., & Inoue, M. 1995, Nature, 373, 127
Mulchaey, J. S., Regan, M. W., & Kundu, A. 1997, ApJS, 110, 299
Nair, P. B. & Abraham, R. G. 2010, ApJS, 186, 427
Nakai, N., Inoue, M., Miyazawa, K., Miyoshi, M., & Hall, P. 1995, PASJ, 47, 771
Narayan, R. & Bartelmann, M. 1995, Proceedings of the 1995 Jerusalem Winter School, Formation of Structure in the Universe, ed. A. Dekel & J. P. Ostriker (Cambridge University Press)
Peck, A. B., Henkel, C., Ulvestad, J. S., Brunthaler, A., Falcke, H., Elitzur, M., Menten, K. M., & Gallimore, J. F. 2003, ApJ, 590, 149
Riess, A. G., Macri, L. M., Hoffmann, S. L., Scolnic, D., Casertano, S., Filippenko, A. V., Tucker, B. E., Reid, M. J., Jones, D. O., Silverman, J. M., Chornock, R., Challis, P., Yuan, W., Brown, P. J., & Foley, R. J. 2016, ApJ, 826, 56
Schawinski, K., Urry, C. M., Virani, S., et al. 2010, ApJ, 711, 284
Springob, C. M., Haynes, M. P., Giovanelli, R., & Kent, B. R. 2005, ApJS, 160, 149
Stanford, S. A. & Balcells, M. 1990, ApJ, 355, 59
Tarchi, A., Henkel, C., Peck, A. B., & Menten, K. M. 2002, A&A, 389, L39
Tarchi, A., Henkel, C., Peck, A. B., & Menten, K. M. 2002, A&A, 385, 1049
Tarchi, A., Castangia, P., Columbano, A., Panessa, F., & Braatz, J. A. 2011, A&A, 532, A125
Tarchi, A., Castangia, P., Henkel, C., Surcis, G., & Menten, K. M. 2011, A&A, 525, A91
Theureau, G., Hanski, M. O., Coudreau, N., Hallet, N., & Martin, J.-M. 2007, A&A, 465, 71
Vader, J. P., Frogel, J. A., Terndrup, D. M., & Heisler, C. A. 1993, AJ, 106, 1743
de Vaucouleurs, G., de Vaucouleurs, A., Corwin, H. G., Buta, R. J., Paturel, G., & Fouque, P. 1991, Third Reference Catalogue of Bright Galaxies (RC3), Springer-Verlag: New York
Zakamska, N. L., Strauss, M. A., Krolik, J. H., et al. 2003, AJ, 126, 2125
Zhu, G., Zaw, I., Blanton, M. R., & Greenhill, L. J. 2011, ApJ, 742, 73